Journal of Solid State Chemistry 183 (2010) 144–149

Contents lists available at ScienceDirect

Journal of Solid State Chemistry

journal homepage: www.elsevier.com/locate/jssc

Carbon nanotube—chalcogenide glass composite

Stepan Stehlik [a], Jiri Orava [a], Tomas Kohoutek [a], Tomas Wagner [a], Miloslav Frumar [a], Vitezslav Zima [b], Toru Hara [c], Yoshio Matsui [c], Kazuyuki Ueda [d], Martin Pumera [e,*]

[a] Department of General and Inorganic Chemistry, Faculty of Chemical Technology, University of Pardubice, Legion's sq. 565, 53210 Pardubice, Czech Republic
[b] Joint Laboratory of Solid State Chemistry of the Institute of Macromolecular Chemistry Academy of Sciences, University of Pardubice, Studentska 84, 52310 Pardubice, Czech Republic
[c] High-Voltage Electron Microscopy Station, National Institute for Materials Science, 1-1 Namiki, Tsukuba, Ibaraki 305-0044, Japan
[d] Nano High Tech Research Center, Toyota Technological Institute, Nagoya 468-8511, Japan
[e] International Center for Materials Nanoarchitectonics and Biomaterials Center, National Institute for Materials Science, 1-1 Namiki, Tsukuba, Ibaraki 305-0044, Japan

ARTICLE INFO

Article history:
Received 3 July 2009
Received in revised form
26 October 2009
Accepted 1 November 2009
Available online 10 November 2009

Keywords:
Carbon nanotubes
Chalcogenide glasses
Ion conductivity
Composites

ABSTRACT

This article describes the preparation of multi-walled carbon nanotube—chalcogenide glass composite by direct synthesis and the melt-quenching method. The carbon nanotubes—chalcogenide glass composite was characterized by high-resolution transmission electron microscopy (HRTEM), TEM/energy-dispersive X-ray spectroscopy, low energy electron excited X-ray spectroscopy, Raman spectroscopy, spectroscopic ellipsometry, microhardness, and impedance spectroscopy. CNTs–$AgAsS_2$ glass composite possess highly increased ionic conductivity, from $\sigma_{25\,^{\circ}C}=4.38\pm0.0438\times10^{-6}$ to $\sigma_{25\,^{\circ}C}=6.57\pm0.0657\times10^{-6}\,S\,cm^{-1}$ and decreased refractive index from $n=2.652$ to 2.631 at the wavelength $\lambda=1.55\,\mu m$.

1. Introduction

Chalcogenide glasses have been widely studied due to their interesting and unique electrical and optical properties [1–4]. If undoped, chalcogenide glasses belong to a large family of vitreous semiconductors usually having p-type conductivity [5]. Chalcogenide glasses doped with metals (such as Ag, Cu, Li) [6–8] or their compounds (i.e., AgI, CuS, Li_2S) behave like ionic conductors or even fast ionic conductors (FIC) [9,10] having $\sigma > 10^{-7}\,S\,cm^{-1}$. The study of the ion conductivity of such glasses is extremely important since these glasses are widely used in many existing applications, in particular as parts of solid state batteries [11] and highly selective and sensitive electrochemical electrodes (i.e., Ag^+, S^{2-}, Se^{2-}, etc.) [12,13]. Chalcogenide ionic glass conductors usually consist of: (i) a network former (sulfides or selenides, e.g., As_2S_3, GeS_2, Ga_2S_2, $GeSe_2$), which are covalent compounds that generally form glass easily, (ii) a network modifier (e.g., Ag_2S, Li_2S, Cu_2S), which are usually compounds with significant ionic features that do not form glass by themselves but can easily react with a glass former and become incorporated in its network, and (iii) a doping element or salt (e.g., Ag, AgI, LiI), which can be introduced into a vitreous network only if the network already contains a former and a modifier [1].

Carbon nanotube (CNT)-doped materials have an enormous potential in a wide variety of applications [14]. CNTs can dramatically alter the mechanical, optical, thermal, electrical, and electrochemical properties of composite materials at surprisingly low levels of doping [14–16]. This has an enormous impact on a wide variety of potential applications, such as reinforced materials, energy storage devices, sensors, and actuators, just to name a few [14–16]. CNTs are incorporated in polymer matrixes [15] or inorganic matrixes, such as silicates or metals [17,18]. Surprisingly, there has been no report on the CNTs–$AgAsS_2$ glass composite. Including of CNTs in to ion-conductive chalcogenide glasses is expected to change their physicochemical properties due to the incorporation into the glass network by the introduction of: (i) a lighter element (lower atomic weight of carbon vs. Ag, As, and S) leading to a change in the optical properties and a consequent decrease in the refractive index; (ii) highly oriented and covalently bonded structures of CNTs resulting in increased hardness, which is expected to improve the mechanical properties of $AgAsS_2$ glass; (iii) crystalline, highly conducting structures, which are expected to increase electron conductivity; and (iv) one-dimensional structures such as CNTs, which are expected to increase ion conductivity.

In this article, we show that CNTs–$AgAsS_2$ glass composite showed a significant increase in its ion conductivity and a simultaneous decrease of the activation energy of the Ag^+ ion conductivity.

* Corresponding author. Fax: +81 29 860 4714.
E-mail address: pumera.martin@nims.go.jp (M. Pumera).

0022-4596/$ - see front matter © 2009 Elsevier Inc. All rights reserved.
doi:10.1016/j.jssc.2009.11.002

2. Experimental section

Materials: Multiwall carbon nanotubes (MWCNTs; length, 7–20 μm; o.d., 90 nm; i.d., 3 nm; MWCNT content >90%; metal catalyst (Fe) content, 3 ppm) [19], Ag, As, and S (purity of 99.999%) were from Sigma-Aldrich.

Synthesis: The primary $AgAsS_2$ glass was synthesized in an evacuated (10^{-3} Pa) and sealed silica ampoule from the elements of 5 N purity. The ampoule was kept in a rocking furnace at 950 °C for 12 h to ensure good homogenization. After the ampoule was removed from the furnace, it was air-cooled to solidify the contents. Some of this glass was further used for synthesizing the CNTs–$AgAsS_2$ glass composite and the rest served as a standard material to compare the physical properties of pure $AgAsS_2$ with the CNTs–$AgAsS_2$ glass composite. The CNTs–$AgAsS_2$ glass composite was synthesized as follows. Pure $AgAsS_2$ was crushed in a mortar producing a fine powder, which was then mixed with an appropriate amount of MWCNTs (0.5 at%) and introduced into the silica ampoule, which was subsequently evacuated and sealed. The synthesis lasted for 16 h at 600 °C. After synthesis, the CNTs–$AgAsS_2$ glass composite was cooled in air and annealed at 130 °C for 3 h.

Apparatus: A Hitachi H-1500 high-resolution transmission electron microscope operating at 800 kV was used to obtain BF (bright field) and HRTEM images as well as electron diffraction patterns. A JEOL 2010F transmission electron microscope operating in STEM mode, 200 kV, was employed to obtain EDX data as well as TEM images. A low energy electron excited soft X-ray spectroscope (LEEXS) was used to detect carbon originating from the MWCNTs (multi-walled carbon nanotubes) in the CNTs–$AgAsS_2$ glass composite. The apparatus contained a low energy electron gun to excite the soft X-ray on the specimen

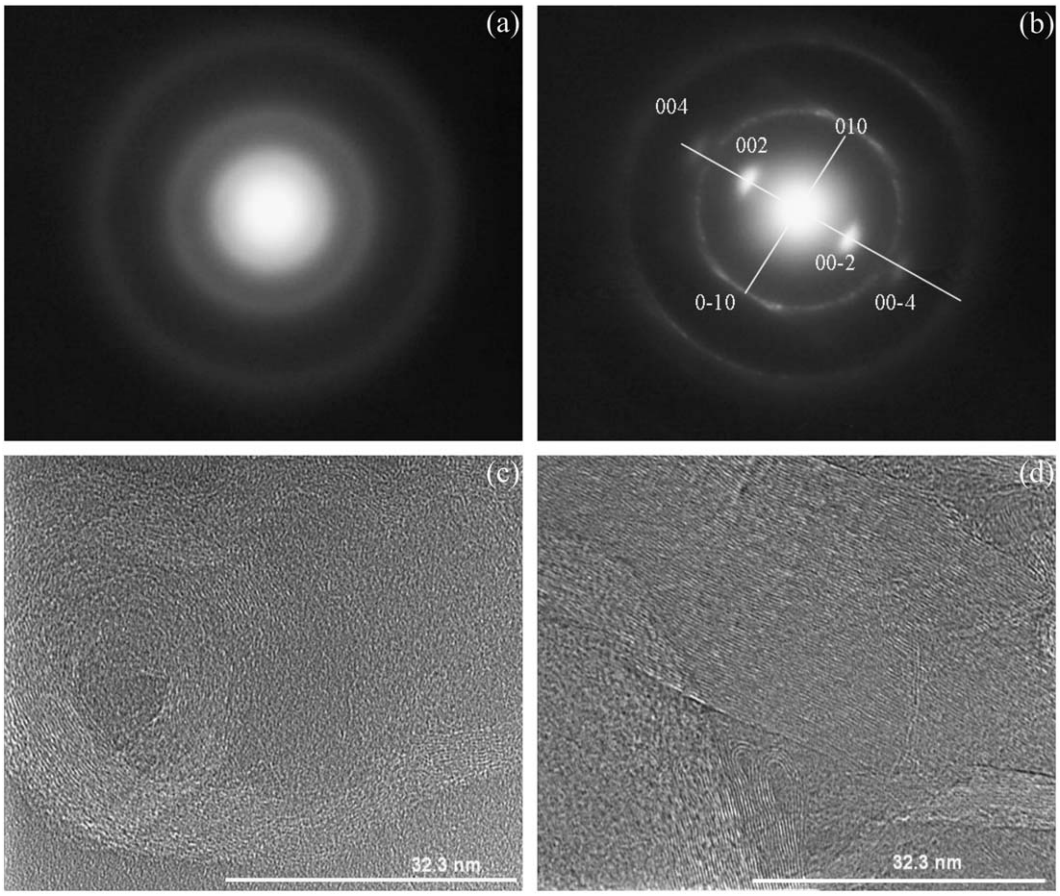

Fig. 1. Electron diffraction patterns of (a) pure $AgAsS_2$ glass and (b) CNTs–$AgAsS_2$ glass composite. (c, d) HRTEM images of MWCNTs in $AgAsS_2$ glass.

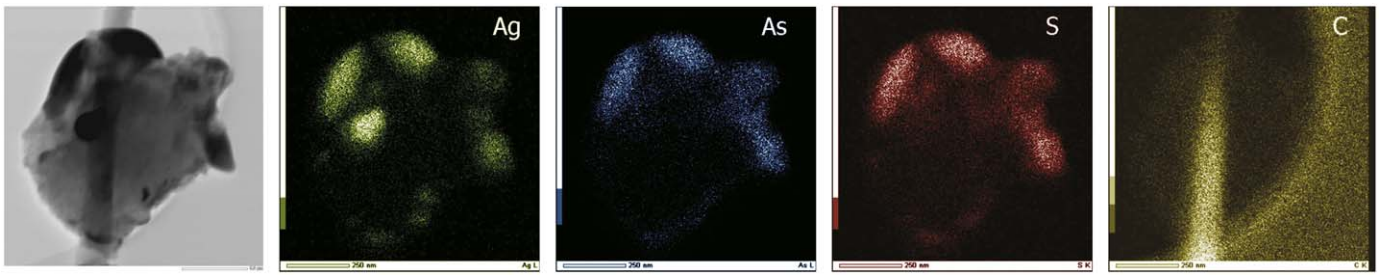

Fig. 2. TEM/EDX analysis of CNTs–$AgAsS_2$ glass composite showing elemental mapping of elements Ag, As, S, and C.

surface ranging from 100 eV to 3 keV and simultaneously to perform low energy electron diffraction (LEED) [20]. Raman spectra were recorded at room temperature with a Fourier transform (FT) Raman spectrometer (Bruker model IFS/FRA 106) using a backscattering method with a Nd:YAG laser (λ = 1064 nm) as an excitation source having an output power of 50 mW. The

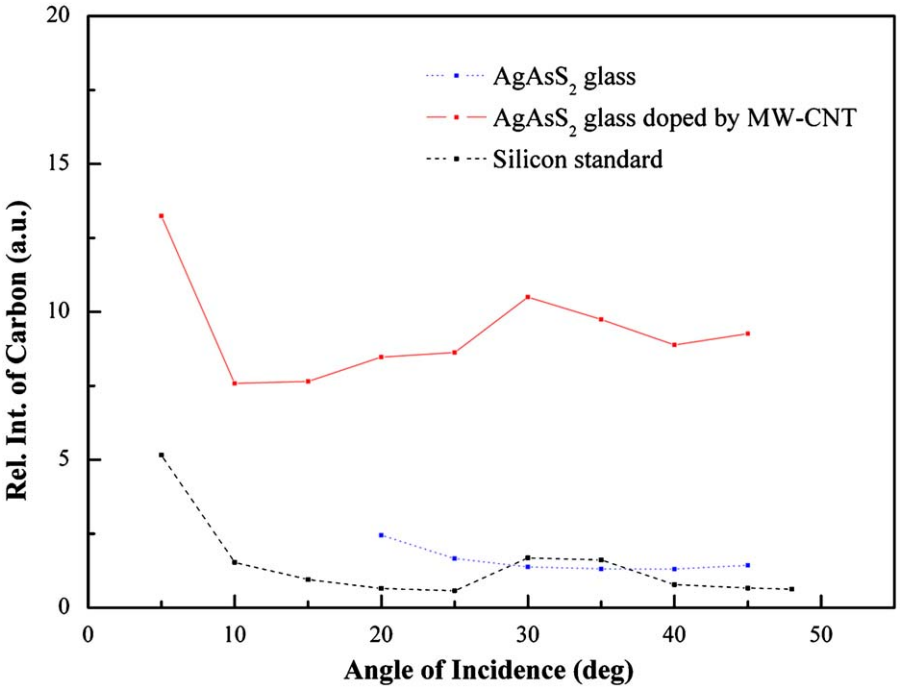

Fig. 3. LEEX analysis of CNTs–$AgAsS_2$ glass composite in comparison with pure $AgAsS_2$ glass and Si standard.

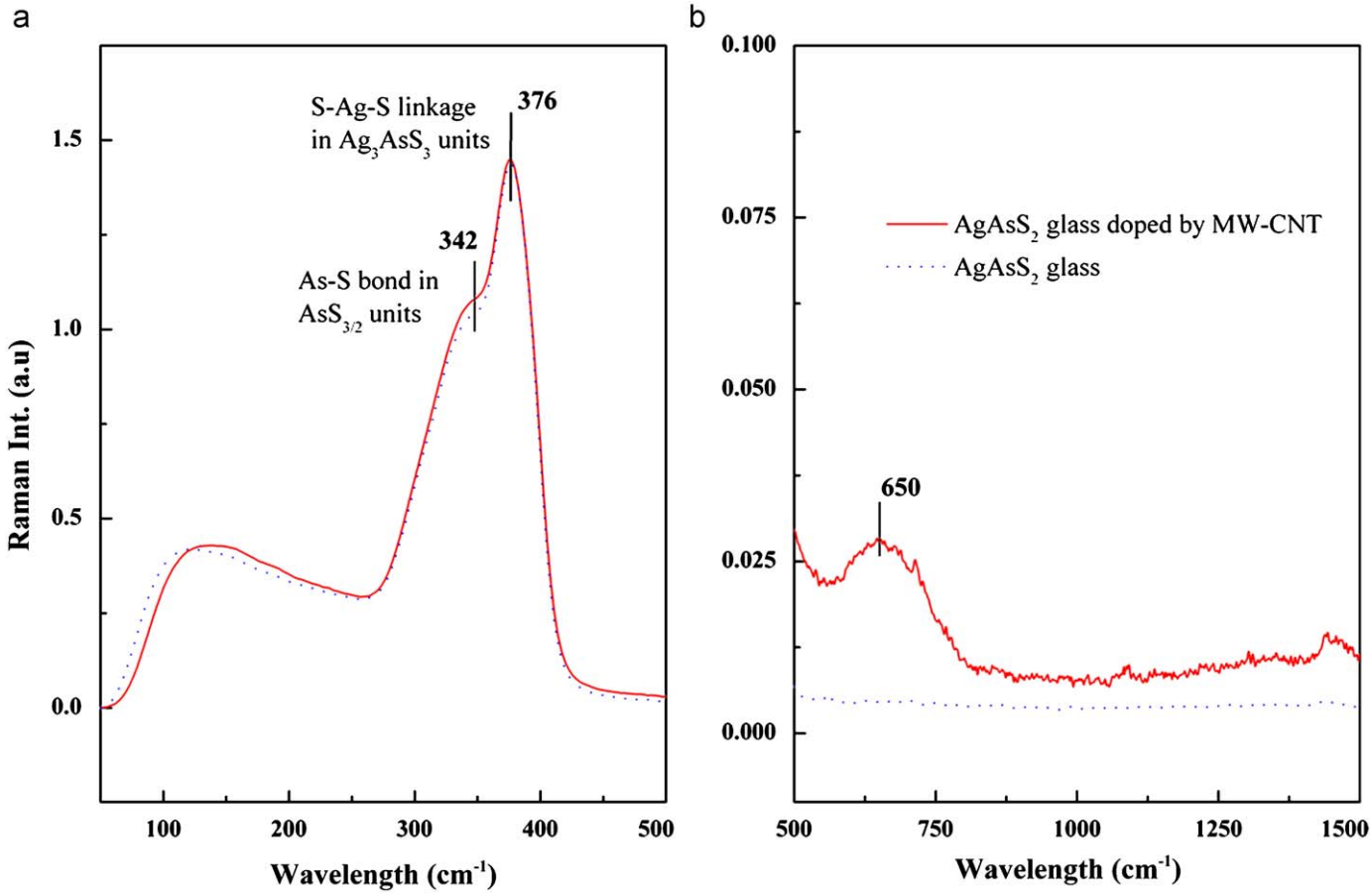

Fig. 4. Raman spectra of pure and CNTs–$AgAsS_2$ glass composite.

resolution of the Raman spectrometer was 1 cm^{-1}, 100 scans recorded. Variable angle spectroscopic ellipsometry (VASE) from J.A. Woollam Co. (WVASE v3.668 software) was used to investigate the optical functions of pure and CNTs–$AgAsS_2$ glass composite. The ellipsometry parameters, Ψ, Δ, were recorded in the range of 300–2300 nm at angles 60–70° with steps of 5°. The accuracy in determination of the refractive index was 0.001. All impedance spectroscopy experiments and potentiostatic measurements were carried out by means of an Autolab PGStat 12 electrochemical analyzer equipped with an FRA2 module. A Julabo MC-4 heating circulator was used to control the temperature. The temperature interval of the electrical measurements was 25–100 °C and the frequency range was 1 MHz–0.1 Hz. The potentiostatic measurements were made at 25 °C under a voltage of 0.1 V in the time interval of 0–250 000 s. The σ_{dcp}/σ_{dc} ratio expresses the residual vs. total conductivity ratio and it determines whether the conductivity is predominantly ionic or electronic (hole). Vickers microhardness was measured using a conventional Vickers diamond pyramid with an apex angle of 136°. We used the weight with a force of F=0.78453 N for 10 s and measured the length of the diagonals of the created indentations (n=3).

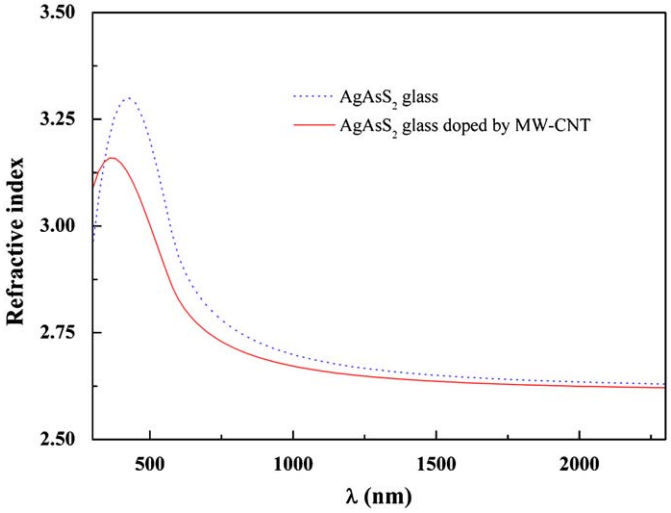

Fig. 5. Spectral dependence of index of refraction.

3. Results and discussion

Chalcogenide $AgAsS_2$ bulk glass was prepared by the conventional melt-quenching technique from pure elements. Transmission electron microscopy was used to examine the structure of the CNTs–$AgAsS_2$ glass composite. Fig. 1 shows electron diffraction and corresponding images of (a) pure $AgAsS_2$ and (b) CNTs–$AgAsS_2$ glass composite. The electron diffraction of pure $AgAsS_2$ is characteristic for amorphous materials. However, the electron diffraction from the CNT containing region of the CNTs–$AgAsS_2$ glass composite shows a diffraction spots typical for CNT materials. The Figs. 1c and d show that the incorporated CNTs are bent, probably due to strains arisen from the synthesis, quenching and solidification of the glass. In these figures, we also observed that the diameter of the multi-wall CNTs is diminished. This was caused by partial destruction of the outer shells of these MWCNTs. The detailed investigation of these changes in the structure of MWCNTs will be a topic of our next studies. Further insight into the structure of the CNTs–$AgAsS_2$ glass composite was obtained by scanning TEM/EDX analysis (Fig. 2). Elemental distribution profiles of silver, arsenic, and sulfur matched and showed maxima at both sides of the carbon nanotubes. The presence of CNTs in the CNTs–$AgAsS_2$ glass composite was also evident from our LEEX measurement [20] (Fig. 3), where a relatively greater concentration of carbon most probably coming from MWCNT in CNTs–$AgAsS_2$ glass composite is shown in comparison with the pure $AgAsS_2$ glass and Si standard.

Raman spectra of the pure $AgAsS_2$ glass and CNTs–$AgAsS_2$ glass composite are shown in Fig. 4. Two prominent peaks at 342 and 376 m^{-1} correspond to pyramidal $AsS_{3/2}$ and –S–Ag–S– linkages in Ag_3AsS_3 units [21]. The CNT adding induced increase in the Raman activity of the mid-frequency ~650 cm^{-1} is related to a

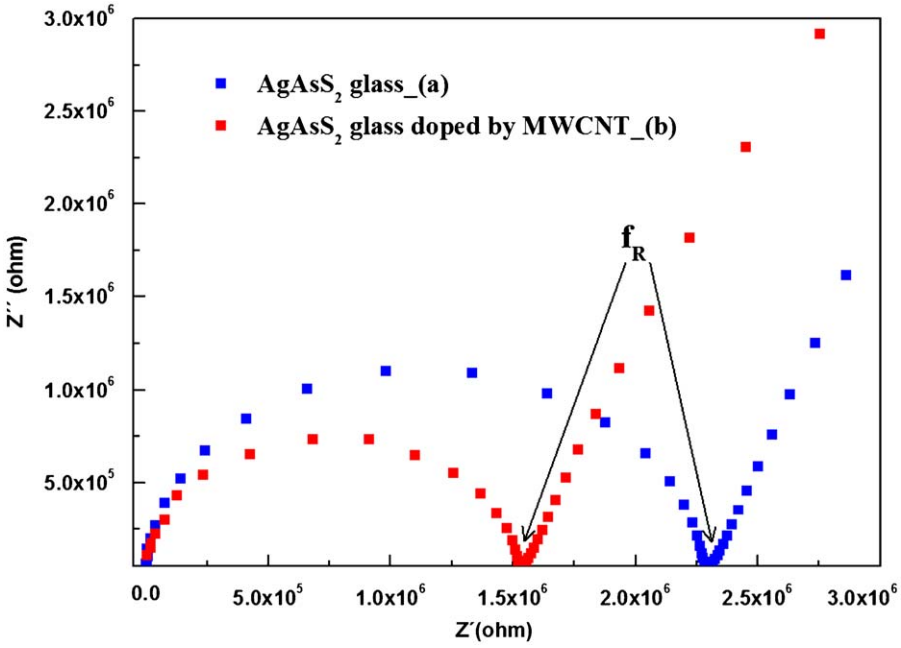

Fig. 6. Impedance spectra of (a) pure and (b) CNTs–$AgAsS_2$ glass composite.

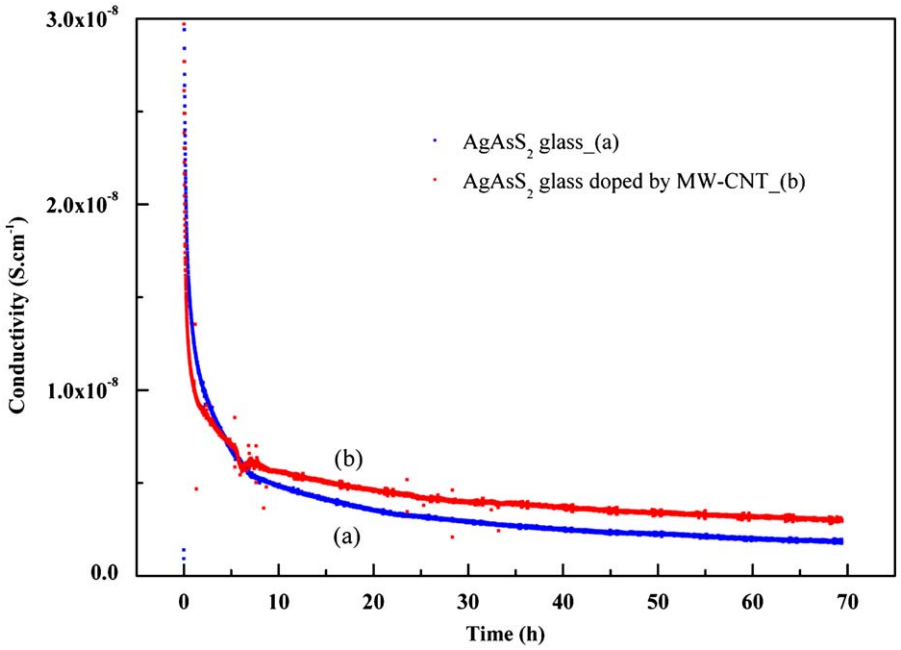

Fig. 7. *Conductivity* vs. *time* dependence potentiostatic curves of (a) pure and (b) CNTs–$AgAsS_2$ glass composite.

Table 1
Comparison of main electric properties $\sigma_{25\,^\circ C}$, E_a, σ_{dcp}/σ_{dc}, and vickers microhardness of pure and CNTs–$AgAsS_2$ glass composite.

Sample	Conductivity$\sigma_{25\,^\circ C}$ (S cm^{-1})	Activation energy, E_a (eV)	σ_{dcp}/σ_{dc}	Wickers microhardness (Pa)
$AgAsS_2$ glass	$4.38 \pm 0.0438 \times 10^{-6}$	$0.401 \pm 2.32 \times 10^{-3}$	0.043	$9.80 \pm 0.098 \times 10^{8}$
CNTs–$AgAsS_2$ glass composite	$6.57 \pm 0.0657 \times 10^{-6}$	$0.366 \pm 3.88 \times 10^{-3}$	0.046	$1.13 \pm 0.0113 \times 10^{9}$

breakdown in the pristine nanotube selection rules associated with the adding and carbon nanotube deformation [22]. This is consistent with the TEM data showing significant deformation of the CNTs incorporated in the $AgAsS_2$ glass.

Consequently, we investigated the influence of the CNT adding to the $AgAsS_2$ glass upon its optical and electrical properties. The change of the optical properties of CNTs–$AgAsS_2$ glass composite is shown in Fig. 5 by an apparent decrease of the refractive index value of ~0.021, i.e., from n=2.652 to 2.631, compared to the pure $AgAsS_2$ glass, both calculated from spectroscopic ellipsometry measurements for the wavelength λ=1.55 μm, which is typically used as a reference value [23]. The index decrease is due to introduction of the lighter element, i.e., carbon from the CNTs, into the network of heavier elements present in chalcogenide glass.

Fig. 6 shows typical impedance spectra of pure $AgAsS_2$ glass and CNTs–$AgAsS_2$ glass composite. Nyquist plots representing typical spectra of ionic conductors consisted of a high-frequency arc (or its part) and a low-frequency tail [24], where the arc is connected with the properties of the sample and the tail with the electrolyte–electrode interface. The point marked f_R is the frequency at which the imaginary part of impedance Z'' reaches its minimum and represents a transition between the high-frequency semicircle and the low-frequency tail, i.e., the frequency at which the polarization on the electrodes occurs due to a space charge accumulation at the sample–electrode interface. The sample conductivity at 25 °C, $\sigma_{25\,^\circ C}$, and activation energy of ion conductivity, E_a, were calculated from Arrhenius law:

$$\sigma = \frac{\sigma_0}{T}\exp\left(-\frac{E_\sigma}{kT}\right) \quad (1)$$

where σ_0 is the pre-exponential factor, E_σ is the activation energy of conductivity, k is the Boltzmann constant, and T is temperature. A significant increase of ion conductivity is shown for CNTs–$AgAsS_2$ glass composite as is obvious from the decreased semicircle radius. We found a 50% increase in $\sigma_{25\,^\circ C}$ conductivity, i.e., from 4.38×10^{-6} to 6.57×10^{-6} S cm^{-1} and a 10% decrease of activation energy E_σ, i.e., from 0.401×10^{-3} to 0.366×10^{-3} eV, for CNTs–$AgAsS_2$ glass composite compared with the pure glass. We assume that the increase in ion conductivity is due to a decrease in the energetic barrier for Ag^+ ion transport in the glass network because some of the ions can travel inside (if some CNTs have open ends or defects on their walls enabling the ions to enter the tubes) or along the CNTs. The Ag^+ diffusion along conducting substrate was proved to be enhanced due to space charge lowering [25]. It means the Ag^+ ions can move more rapidly through the structure of the glass.

Fig. 7 shows the DC potentiostatic curves of pure $AgAsS_2$ glass and CNTs–$AgAsS_2$ glass composite. The measured I vs. t curves were recalculated to σ vs. t curves taking into account the dimensions of the samples. After 3 days of measurement, the residual conductivity of the samples showed values that were near equilibrium. The ion conductivity vanished after approximately 5 h. The CNTs–$AgAsS_2$ glass composite had slightly higher residual conductivity than the pure glass most

probably due to the presence of CNT in the glass. Table 1 summarizes all results determined from impedance and DC potentiostatic measurements together with the values of microhardness, which increased in the case of CNT-doped $AgAsS_2$ glass by about 15%, from 9.80×10^8 to 1.13×10^9 Pa. This increase is probably caused by the presence of hardly deformable covalent C–C bonds in the MW-CNT which are present in the CNTs–$AgAsS_2$ glass composite.

4. Conclusions

We have successfully prepared ion-conductive CNTs–$AgAsS_2$ glass composite at relatively low temperature. To the best of our knowledge, this paper represents the first example of conductivity study of CNT–chalcogenide glass composite. Despite a low level of CNTs concentration and a slight change in the CNTs morphology in the glass network, the presence of CNTs brought about rapid improvement of silver ion transport and conductivity, which is expected to offer significant benefits for future battery applications. A likely prospect seems to be the adding of single-walled CNTs in to ion-conductive glasses, which is expected to further enhance ion transport due to the possibility of tailoring the diameter of single-walled CNTs.

Acknowledgments

This work was supported by the Ministry of Education, Youth and Sports (Research Centre LC 523 project), Czech Science Foundation (projects GA 203/08/P204 and GA 203/08/0208). This work was also supported in part by the World Premier International Research Center (WPI) Initiative on Materials Nanoarchitectonics, MEXT, Japan (M.P.)

References

[1] D.B. Mitzi, Adv. Mater. 21 (2009) 3141.
[2] M. Frumar, T. Wagner, Curr. Opin. Sol. State Mater. Sci. 7 (2003) 117.
[3] T. Wagner, S.O. Kasap, Phil. Mag. B: Phys. Cond. Matter 74 (1991) 667.
[4] M. Frumar, A.P. Firth, A.E. Owen, Phil. Mag. B: Phys. Cond. Matter 50 (1984) 463.
[5] S.R. Elliott, Adv. Phys. 36 (1987) 135.
[6] P. Boolchand, W.J. Bresser, Nature 410 (2001) 1070.
[7] A.V. Kolobov, S.R. Elliott, Adv. Phys. 40 (1991) 625.
[8] M. Ohto, M. Itoh, K. Tanaka, J. Appl. Phys. 77 (1995) 1034.
[9] M. Mitkova, Y. Wang, P. Boolchand, Phys. Rev. Lett. 83 (1999) 3848.
[10] W. Yao, S.W. Martin, Solid State Ionics 178 (2008) 1777.
[11] M.D. Ingram, in: M. Cable, J.M. Parker (Eds.), High-Performance Glasses, Chapman and Hall, New York, 1992 (Chapter 7).
[12] M.N. Kozicki, M. Mitkova, M. Park, M. Balakrishnan, C. Gopalan, Superlattice. Microst. 34 (2003) 459.
[13] C. Cali, D. Foix, G. Taillades, E. Siebert, D. Gonbeau, A. Pradel, M. Ribes, Mater. Sci. Eng. 21 (2002) 3.
[14] P.M. Ajayan, J.M. Tour, Nature 447 (2007) 1066.
[15] K. Kobashi, T. Villmow, T. Andres, L. Häußler, P. Pötschke, Smart Mater. Struct. 18 (2009) 035008.
[16] M. Pumera, S. Sanchez, I. Ichinose, J. Tang, Sensor. Actuator. B 123 (2007) 1195.
[17] T. Seeger, Th. Kohler, Th. Frauenheim, N. Grobert, N. Ruhle, M. Terrones, G. Seifert, Chem. Comm. 34 (2002).
[18] M. Reibold, P. Paufler, A.A. Levin, W. Kochmann, N. Pätzke, D.C. Meyer, Nature 444 (2006) 286.
[19] T. Kolodiazhnyi, M. Pumera, Small 4 (2008) 1476.
[20] K. Ueda, Y. Yoshikawa, J. Surf. Sci. Nanotech. 4 (2006) 443.
[21] G. Lukovski, F.L. Geils, R.C. Keezer, The Structure of Non-Crystalline Materials, Taylor and Francis, London, 1977 127pp.
[22] A.M. Rao, S. Bandow, E. Richter, P.C. Eklund, Thin Solid Films 331 (1998) 141.
[23] M. Bass, Handbook of Optics, vol. 2, Optical Society of America, New York, 1994.
[24] J.R. Macdonald, Impedance Spectroscopy Emphasising Solid Materials and Systems, Wiley, New York, 1987.
[25] M. Frumar, A.P. Firth, A.E. Owen, The mechanism of photoenhanced silver dissolution in amorphous As-S layers, in: E. Fachrivateva, A. Buroff (Eds.), Proceedings of the Conference "Amorphous Semiconductors-84", vol. 1, Bulgarian Academy of Sciences, Sofie, 1984, pp. 216–218.